Design of Inline Waveguide Filters with Frequency-Variant Couplings Producing Transmission Zeros

Giuseppe Macchiarella, *Fellow, IEEE*, Gian Guido Gentili, Nicolò Delmonte, *Student Member, IEEE*, Lorenzo Silvestri, *Member, IEEE*, and Maurizio Bozzi, *Fellow, IEEE*

***Abstract*—A general design procedure for inline waveguide filters with frequency-variant couplings (FVC) is presented. The goal of the design is the introduction of transmission zeros in the filter response. The filter design starts with the synthesis of a low-pass prototype with FVC, adopting a method recently appeared in the literature. The low-pass prototype is then de-normalized to obtain an equivalent circuit of the filter suitable for waveguide implementation. The last step of the design consists in the dimensioning of the physical structure of the filter, including the frequency-dependents couplings, by exploiting the equivalence with the synthesized equivalent circuit. The design procedure can be applied independently on the specific structure implementing the FVCs. In the case of narrow-band filters, the resulting structure may not require any further refinements by means of numerical optimization based on full-wave modelling. A design example illustrates the details of the procedure implementation. The validation of the procedure is presented through the design and fabrication of a substrate integrated waveguide (SIW) filter with two coincident transmission zeros.**

***Index Terms*—Frequency-dependent couplings, singlet, substrate integrated waveguide, waveguide filters.**

I. INTRODUCTION

MICROWAVE FILTERS exhibiting transmission zeros in the frequency response are more and more required in most communication systems. However, the classical solutions for introducing transmission zeros in the filter response are often not satisfying, because they may require an unacceptable increase of the overall filter size or because they make the resulting structure complex to be realized (and therefore more expensive). For this reason, the recent research in the microwave filters area has been addressed to identify alternative solutions, characterized by simple topologies and by an easy control of the transmission zeros. Today, one of these solutions is based on the use of frequency-variant couplings (FVC), resonating at the frequency of the transmission zeros. It must be observed that, strictly speaking, all coupling structures used in microwave filters are frequency dependent. However, it is usual practice in the design of classical coupled-cavity filters to discard this dependence when the normalized bandwidth is small. This assumption made the development of the most popular design techniques today available for microwave filters possible [20]. Such an approach, however, becomes less and less accurate with the increase of the filter bandwidth. A possible solution to improve the design accuracy of broadband microwave filters is to include FVCs in the design procedures [1]. Our work, however, focuses on the other reason that has made FVCs so popular today: the possibility of introducing transmission zeros (TZs) in the filter response by imposing zeroing of the couplings at TZ frequencies. Such a solution for generating TZs was first proposed in 1999 [2] and since then the use of resonant FVCs in microwave filters has become a convenient choice for realizing compact and selective devices [3]-[14]. However, most of the works appeared in the literature in the past years approached the design of this filter class empirically or by means of numerical optimization. Only very recently more robust design techniques, based on the coupling matrix synthesis, have appeared [15]-[19].

This work is focused on a synthesis-based design approach for waveguide FVC filters with inline topology exhibiting transmission zeros in the response. This is a very interesting solution for realizing compact filters with transmission zeros, easy to fabricate and tune. The design of this type of waveguide filters was initially carried out by optimization [2]-[4]. More recently, research efforts have been taken to develop more systematic and accurate design approaches. In [17] a novel synthesis procedure is proposed, allowing the evaluation of coupling and capacitance matrices of inline filters with transmission zeros (no practical implementations for waveguide filters are however discussed).

A general design approach for waveguide filters with dispersive coupling elements was introduced in [19]. The proposed method is based on an iterative procedure allowing the extraction of the frequency dependent part of the coupling matrix by means of full wave simulations of the physical coupling structures. Although accurate design results are shown, this method seems rather involved and not easy to be implemented.

The design approach proposed in this work starts with the synthesis of a normalized prototype including FVCs. The

Manuscript received Nov. 30, 2020; revised Feb. 12, 2021.

G. Macchiarella and G.G. Gentili are with Dipartimento di Elettronica, Informazione e Bioingegneria, Politecnico di Milano, 20133 Milano, Italy (e-mail: giuseppe.macchiarella@polimi.it).

N. Delmonte, L. Silvestri, and M. Bozzi, are with the Department of Electrical, Computer, and Biomedical Engineering, University of Pavia, 27100 Pavia, Italy (e-mail: nicolo.delmonte01@universitadipavia.it; lorenzo.silvestri01@universitadipavia.it; maurizio.bozzi@unipv.it).

synthesis method in [17] provides the normalized coupling and capacitances matrices of the inline topology and allows up to *N*-1 transmission zeros in the frequency response (where *N* is the order of the filter). The normalized prototype is then de-normalized and further manipulations are introduced so that the resulting bandpass equivalent circuit of the filter is suitable for waveguide implementation. An original procedure has been adopted in this phase, which allows transforming the frequency-dependent impedance inverters, generated by the synthesis, into shunt connected series resonators (practically implementable with physical structures). Moreover, the interaction between the structures introducing the transmission zeros and the main resonators of the filter is taken into account by the procedure. The resulting lumped-element circuit is finally modified by replacing the main (series) resonators with waveguide equivalent cavities. Since the latter are not strictly equivalent to the original lumped resonators, an optimization of the resulting circuit may be necessary to restore the equiripple response in the passband. The optimization is however very fast in this case, because it is carried out on the equivalent circuit and because the starting point is generally not too far from the desired response. The design procedure then proceeds with the physical implementation of the coupling structures. Those which are frequency independent are realized with the usual inductive irises. For the FVCs possible structures are discussed, also allowing the placement of transmission zeros very close to the passband. The selected FVC structure resonates at the frequency of the transmission zero and must exhibit the same equivalent slope parameter of the synthesized lumped resonator. The dimensioning of the coupling structures is carried out separately, by imposing the same scattering parameters versus frequency of the corresponding lumped elements in the filter equivalent circuit. The last step of the design procedure is the correction of the cavities length to account for the loading effects produced by the coupling elements.

We would like to underline the novelty of the design approach introduced here. Unlike many synthesis solutions in the literature, our method is based on the synthesis of a very accurate equivalent circuit and it allows for the dimensioning of the filter structure element by element (exploiting full wave simulations). The overall accuracy of the design is very high: in many cases, further adjustments may not be required after the initial dimensioning.

The synthesis of the equivalent circuit of the filter with FVCs is described in Section II, while the derivation of an equivalent circuit suitable for waveguide implementation of the filter is discussed in Section III. Section IV discusses the filter dimensioning and shows possible practical implementation of the adopted FVCs. Finally, the experimental validation of the proposed design approach is presented in Section V through the design and manufacturing of a filter in SIW technology.

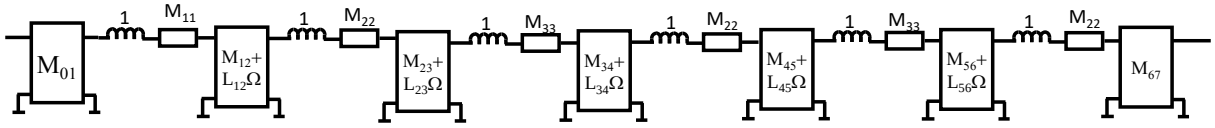

Fig. 1. Synthesized prototype with frequency-dependent impedance inverters. The prototype is characterized by *M* (coupling matrix) and *L* (inductance matrix). Note that some impedance inverters can be frequency-independent (i.e. $L_{k,k+1}$=0)

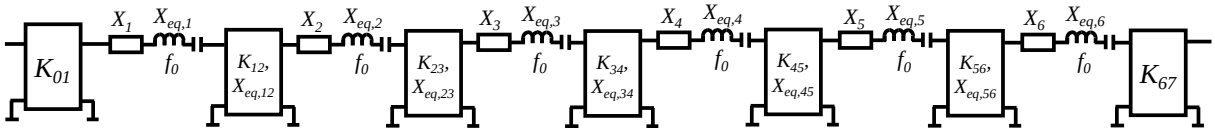

Fig. 2. Bandpass equivalent circuit of the filter. Note that $X_{eq,i}$, X_i, $K_{i,i+1}$ and $Kv_{i,i+1}$ are arbitrary, provided that the coefficient $k_{i,i+1}$ and $kv_{i,i+1}$ defined in (2) are conserved. For frequency-independent inverters $X_{eq,k,k+1}$=0.

II. SYNTHESIS OF INLINE FILTERS WITH TRANSMISSION ZEROS

The design of the waveguide filters here considered starts, as usual, with the synthesis of a low-pass prototype of order *N* in the normalized domain Ω defined by the frequency transformation $\Omega = \left(f/f_0 - f_0/f \right)/B_n$, with f_0 passband center frequency and B_n normalized bandwidth. We assume that N_z transmission zeros are imposed, with N_z<*N*. In the case of FVCs, an effective procedure has been recently published, allowing the evaluation of the coupling (*M*) and capacitance (*C*) matrices of the shunt equivalent circuit of the filter [17]. In the present case, we need the series equivalent circuit for the filter, so we will refer in the following to the coupling (*M*) and inductance (*L*) matrices. Note that the procedure presented in [17] can be used as well: in fact, it does not depend on the meaning assigned to the variable part of the couplings.

Once the characteristic polynomials, defining the filter response, have been evaluated, the procedure in [17] allows to obtain the parameters of the low-pass prototype reported in Fig. 1. Note that the first and last impedance inverters cannot be frequency-dependent, so up to *N*-1 transmission zeros can be introduced in the response. In fact, while the inner inverters do not modify the number of poles of the prototype, it can be verified that introducing a frequency dependence in the first (or last) inverter would increase the number of poles by one, making not synthesizable the assigned polynomial characteristic (of order *N*). When the assigned TZs are less than *N*-1, the position of the inverters extracting the TZs must be specified. All the remaining inverters, in this case, are frequency-independent (as remarked in the caption of Fig. 1).

The following step is the de-normalization, i.e., the transformation of the low-pass prototype into the band-pass equivalent circuit of the filter (Fig. 2). This can be done by replacing the unit inductors in Fig. 1 with series resonators and imposing the same reactance of the series arms in the de-normalized domain. This result is obtained by assigning the inductance of the resonator equal to $1/B_n$ and leaving unchanged the reactances $M_{i,i}$. Because of the linear dependence on Ω, the parameters of the frequency-dependent impedance inverters ($MF_{i,i+1}$) become, after the de-normalization:

$$MF_{i,i+1} = M_{i,i+1} + \frac{L_{i,i+1}}{B_n}\left(\frac{f}{f_0} - \frac{f_0}{f}\right) \tag{1}$$

However, we observe that the de-normalized filter is not unique, due to the presence of the inverters. In fact, we can assign arbitrarily either the equivalent reactance of the resonators ($X_{eq,i}$) or the impedance inverters parameters [$KF_{i,i+1}=K_{i,i+1}+X_{eq,i,i+1}(f/f_0-f_0/f)$], provided that the following universal coefficients (namely the *coupling coefficients*) are preserved

$$k_{i,i+1} = \frac{K_{i,i+1}}{\sqrt{X_{eq,i}X_{eq,i+1}}} = B_n M_{i,i+1}, \quad kv_{i,i+1} = \frac{X_{eq,i,i+1}}{\sqrt{X_{eq,i}X_{eq,i+1}}} = L_{i,i+1},$$
$$k_{01} = \frac{K_{01}^2}{X_{eq,1}} = B_n M_{01}^2, \quad k_{N,N+1} = \frac{K_{N,N+1}^2}{X_{eq,N}} = B_n M_{N,N+1}^2 \tag{2}$$
$$M_{i,i} \rightarrow X_i = X_{eq,i} M_{i,i} B_n$$

Note that $kv_{i,i+1}=0$ for the frequency-independent inverters. Note also that the reactances $M_{i,i}$ are replaced by the frequency-invariant reactances X_i to preserve the resonant frequencies of the series-connected impedances.

The de-normalized band-pass circuit (Fig. 2) is then defined by the parameters $X_{eq,i}$, X_i, $K_{i,i+1}$ and $X_{eq,i,i+1}$ related each other through (2).

The circuit in Fig. 2 can be further manipulated by replacing the impedance inverters with a T equivalent circuit (Fig. 3) [19].

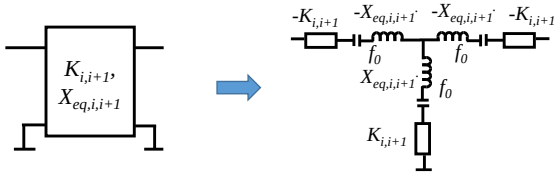

Fig. 3. Equivalent representation of the inverters. $X_{eq,i,i+1}$ represents the equivalent reactance of the series resonators (with resonating frequency equal to f_0). The reactances $K_{i,i+1}$ are frequency-invariant.

After the replacement, the circuit in Fig. 4 is obtained. The first and last inverters are not transformed, because they will be directly implemented in the waveguide filter. Note that not all the shunt reactances include a series resonator. In fact, those derived from frequency-independent inverters are constituted only by the frequency-invariant reactance $K_{i,i+1}$.

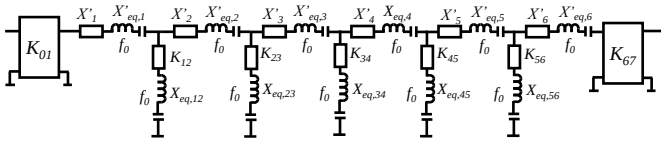

Fig. 4. Equivalent circuit of the bandpass filter after replacing the impedance inverters with their T equivalent circuit. Shunt arms derived from frequency-invariant inverters include the reactance $K_{i,i+1}$ only.

The expressions of the new parameters in Fig. 4 $\left(X'_{eq,i},\ X_{eq,i,i+1},\ X'_i \text{ and } K_{i,i+1}\right)$ are reported in (3)

$$\begin{aligned}
X'_{eq,i} &= X_{eq,i} - kv_{i-1,i}\sqrt{X_{eq,i-1}X_{eq,i}} - kv_{i,i+1}\sqrt{X_{eq,i}X_{eq,i+1}} \\
X'_{eq,1} &= X_{eq,1} - kv_{12}\sqrt{X_{eq,1}X_{eq,2}}, \\
X'_{eq,N} &= X_{eq,N} - kv_{N-1,N}\sqrt{X_{eq,N-1}X_{eq,N}} \\
X'_i &= X_i - K_{i-1,i} - K_{i.i+1} \\
X'_1 &= X_1 - K_{12}, \quad X'_N = X_N - K_{N-1,N} \\
X_{eq,i,i+1} &= kv_{i,i+1}\sqrt{X_{eq,i}X_{eq,i+1}} \qquad i = 1,\ldots N-1 \\
K_{i,i+1} &= k_{i,i+1}\sqrt{X_{eq,i}X_{eq,i+1}} \qquad i = 1,\ldots N-1
\end{aligned} \tag{3}$$

We observe that, assuming $X_{eq,i}$ arbitrarily assigned, all the other parameters of the circuit in Fig. 4 can be derived once the low-pass prototype has been synthesized and the coupling coefficients computed with (2).

It can also be observed that the response of the circuit in Fig. 4 is exactly the one obtained by the polynomial model assumed at the beginning, transformed into the band-pass domain with the previously defined frequency transformation.

To simplify the practical implementation, we can now introduce an approximation (widely adopted in coupled-cavity microwave filters), consisting in removing the series-connected frequency invariant reactance, de-tuning at the same time the resonator, so that the resonance frequency remains unchanged (Fig. 5).

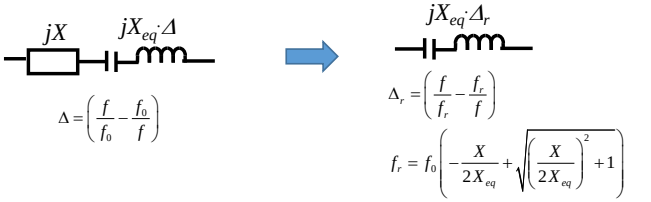

Fig. 5. Removal of frequency-invariant reactance in series with the series resonators.

Note that the slope parameter of the resonator (X_{eq}) is unaffected by the above transformation. As well known, the approximation introduced is in general acceptable for narrow band filters with transmission zeros not too distant from the passband.

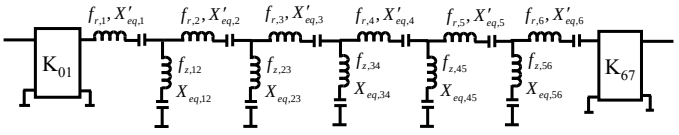

Fig. 6. Final equivalent circuit of the filter with frequency-dependent couplings. In case the coupling $i,i+1$ is not resonating, the series resonator is replaced by the frequency-independent reactance $X_{i,i+1}=K_{i,i+1}$.

The final equivalent circuit of the filter with frequency-dependent couplings is reported in Fig. 6.

The resonating frequencies of the resonators are given by:

$$f_{r,i} = f_0\left(-\frac{X'_i}{2X'_{eq,i}} + \sqrt{\left(\frac{X'_i}{2X'_{eq,i}}\right)^2 + 1}\right), \qquad f_{z,i,i+1} = f_0\left(-\frac{K_{i,i+1}}{2X_{eq,i,i+1}} + \sqrt{\left(\frac{K_{i,i+1}}{2X_{eq,i,i+1}}\right)^2 + 1}\right) \tag{4}$$

Obviously, the resonant frequencies of the shunt connected series resonators coincide with the assigned transmission zeros.

We observe that the original synthesized circuit with ideal frequency-dependent inverters has been transformed into a circuit configuration with only series resonators. In waveguide technology, the horizontal series resonators can be approximated by classical rectangular cavities operating on the TE_{10n} mode. Various solutions exist for implementing the shunt connected (rejection) resonators (e.g., stubs or singlets). In the next sections we will discuss how to perform the synthesis of the circuit in Fig. 6 so as it is compatible with the waveguide implementation.

III. DERIVATION OF THE FILTER EQUIVALENT CIRCUIT

A. *Implementation of main resonators with waveguide cavities*

The first step for designing the waveguide filter is to assign the filter cavities (corresponding to horizontal series resonators in Fig. 6). We assume to implement these resonators by means of rectangular waveguide cavities operating on the TE_{10n} mode. It must be remarked that this equivalence is not exact not only because the cavity is a distributed element. In fact, the 2-port parameters of a transmission line section cannot all coincide with the same parameters of a series connected reactance, not even at a single frequency. In the case however, source and load terminations are much smaller of the characteristic impedance of the line, it can be verified that S_{11} and S_{12} of the line can be approximated by those of a series resonator in a small frequency range around the resonance frequency (where the electrical length of the line is $\theta=n\pi$) [19],[20].

Assuming that this condition is verified, we can then replace the horizontal series resonators in Fig. 6 with waveguide cavities of electrical length $n\pi$ at the resonance frequencies $f_{r,i}$. To do this, the equivalent reactance of the resonators must be equal to the slope parameter of the cavities at the center of the passband (f_0), that is [19]

$$X'_{eq} = \frac{n(\pi/2)}{1-(f_c/f_0)^2} \tag{5}$$

This result can be achieved with suitable values assigned to the equivalent reactances $X_{eq,i}$ of the initially synthesized equivalent circuit (Fig. 2). Such values are the solution of the following non-linear system (derived from (3) and (5)):

$$X'_{eq,i} = X_{eq,i} - \bar{X}_i = \frac{n(\pi/2)}{1-(f_c/f_0)^2} \qquad i = 1,\ldots N \tag{6}$$

with

$$\bar{X}_i = kv_{i-1,i}\sqrt{X_{eq,i-1}X_{eq,i}} + kv_{i,i+1}\sqrt{X_{eq,i}X_{eq,i+1}} \quad i = 2,\ldots N-1$$
$$\bar{X}_1 = kv_{12}\sqrt{X_{eq,1}X_{eq,2}}\ ,\ \bar{X}_N = kv_{N-1,N}\sqrt{X_{eq,N-1}X_{eq,N}} \tag{7}$$

Note that $kv_{i,i+1}$, are known after the synthesis of the prototype (they do not depend on $X_{eq,i}$). Once (6) is solved, $X_{eq,i}$ are known and, by means of (3), we can compute all the shunt reactances, defined by the parameters $K_{i,i+1}$ (if frequency-independent) or $X_{eq,i,i+1}$ (if frequency-dependent). The main series resonators are characterized by the resonating frequencies $f_{r,i}$ in (4). Consequently, the lengths $L_{r,i}$ of the rectangular cavities is given by (v is the light velocity in the medium filling the waveguide):

$$L_{ris,i} = \frac{n(v/2\,f_{r,i})}{\sqrt{1-(f_c/f_{r,i})^2}} \tag{8}$$

It is worth observing that the replacement of the main series resonators with the waveguide cavities produces a degradation of the filter response that is no longer coincident with the one obtained from the polynomial model defining the ideal Chebycheff Characteristic. The response degradation is not easy to quantify *a priori* because it does not depend only on the normalized filter bandwidth (B_n), but also on the loads that each cavity sees at its ends. In general, we can expect that the smaller the normalized bandwidth, the closer the filter response is to the ideal one. In the cases where the discrepancies with the ideal response are large, a circuit optimization may be employed to properly tune the filter response.

B. *Equivalent circuit of the filter*

As explained in Section II, first and last inverters cannot be frequency dependent. They are however replaced by the equivalent circuit in Fig. 7 to make possible their physical implementation.

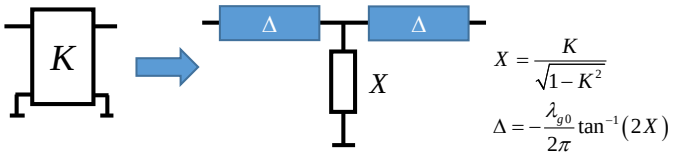

Fig. 7. Equivalent circuit of first and last inverters. λ_{g0} in the waveguide wavelength at the passband center frequency.

Consequently, the first and last couplings are represented by frequency invariant reactances (X_{01} and $X_{N,N+1}$), while the length of first and last cavities becomes (K is K_{01} or $K_{N,N+1}$):

$$L_{ris,i} = \frac{n(v/2\,f_{r,i})}{\sqrt{1-(f_c/f_{r,i})^2}} - \frac{\lambda_{g0}}{2\pi}\tan^{-1}\left(\frac{2K}{\sqrt{1-K^2}}\right) \qquad (i = 1, N) \tag{9}$$

Fig. 8 shows the equivalent circuit of the filter, after the introduction of the waveguide resonators.

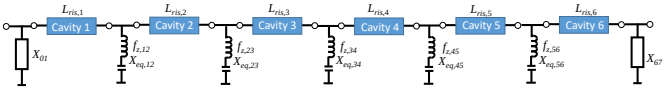

Fig. 8. Equivalent circuit of the filter after the introduction of the waveguide cavities. The rejection resonators are replaced by frequency-invariant reactances of value $X_{i,i+1}=K_{i,i+1}$ for the couplings not introducing a transmission zero.

C. *Examples of equivalent circuit synthesis*

As a first example a rectangular waveguide filter with the following specifications is considered: Center frequency f_0=19.82 GHz; Bandwidth B=240 MHz; Return Loss RL=23 dB; Filter order N=6; Transmission zeros f_z=(19.677 GHz, 19.968 GHz); waveguides cutoff frequency f_c=11.58 GHz. The cavities resonate on TE_{102} mode (n=2 in (5) and (8)).

The synthesis algorithm produces the following de-normalized parameters (the FVCs are assigned to inverters (2,3) and (4,5)): $k_{01}= k_{67}= 0.013336$; $k_{i,i+1}$=[0.0074421, 0.01032, 0.0037339, 0.010126, 0.0077463], $kv_{i,i+1}$=[0, 0.71109, 0, 0.68147, 0]. Using (5) with n=2, the equivalent reactance of all the final resonators is set equal to $X'_{eq} = \pi\left(1-\left(f_c/f_0\right)^2\right)^{-1} = 4.7678$.

Solving the system (6), the equivalent reactances $X_{eq,i}$ of the initial equivalent circuit of the filter are obtained: $X_{eq,i}$=[4.768, 16.503, 16.503, 14.968, 14.968, 4.768].

Using (3) all the parameters of the final equivalent circuit of the filter (Fig. 6) can be derived: $K_{01}=K_{67}=0.2522$, X_{12}=0.066014, X_{34}=0.058685, X_{56}=0.06544, $X_{eq,23}$=11.735, $X_{eq,45}$=10.2005, $f_{z,23}$=19.6767, $f_{z,45}$=19.9678, $f_{r,i}$=[19.958, 19.969, 19.979, 19.9054, 19.942, 19.9566]

Finally, introducing the waveguide resonators and replacing the first and last inverters with the equivalent circuit in Fig. 7, the final scheme of the synthesized filter is obtained (Fig. 9).

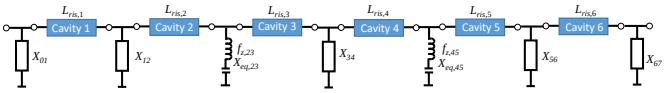

Fig. 9. Final scheme of the synthesized filter. The length of the cavities (operating on TE_{102} mode) are obtained introducing $f_{r,i}$ into (8) and (9): $L_{ris,i}$=[17.7074, 18.4241, 18.4109, 18.5133, 18.4624, 17.7091]mm. Note that the length of first and last cavities includes the contribution from the equivalent circuit of first and last inverters (Fig. 7). The coupling reactances derived from these inverters are $X_{01}=X_{67}$=0.2693).

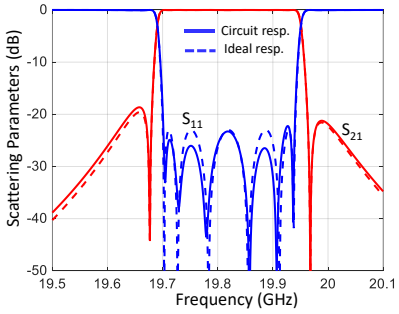

Fig. 10. Response of synthesized equivalent circuit (first example). Solid lines: synthesized circuit (Fig. 9). Dashed lines: Ideal (Chebycheff) response.

The response of the computed equivalent circuit is shown in Fig. 10. As reference, also the ideal Chebycheff response is reported. As can be observed, the discrepancies produced by the replacement of the series resonators with waveguide cavities are in this case negligible (note that the normalized bandwidth of the filter is 1.21%).

The second example concerns a dielectric-filled rectangular waveguide filter with the following requirements: center frequency f_0=5 GHz; Bandwidth B=153.5 MHz; Return Loss RL=17 dB; Filter order N=5; transmission zeros (coincident) f_z=(4.91 GHz, 4.91 GHz); relative dielectric constant of the medium ε_r=2.2; waveguides cutoff frequency f_c=3.37 GHz. The cavities resonate on TE_{101} mode (n=1 in (5) and (8)).

Using the synthesis algorithm, we get the following result (the FVCs are assigned to second (1,2) and fifth (4,5) inverters)

$k_{01}= k_{67}= 0.0106888$

$k_{i,i+1}$=[0.028625, 0.013053, 0.01305, 0.02862],

$kv_{i,i+1}$=[0.7839656, 0, 0, 0.7839656].

The equivalence slope parameter of the cavities is obtained from (5) with n=1:

$$X'_{eq} = \frac{\pi}{2}\left(1-\left(f_c/f_0\right)^2\right)^{-1} = 2.876$$

After solving the system (6) and using (3) we get the final equivalent circuit parameters: $K_{01}=K_{56}= 0.37722$, $X_{23}=X_{34}=$ 0.080769, $X_{eq,12}=X_{eq,45}=$ 10.4366, $f_{z,12}= f_{z,45}$=4.91, $f_{r,i}$=[4.9739, 5.1563, 5.1572, 5.1563, 4.9739]. Finally, replacing the series resonators we get from (8) the following lengths (in mm) for the waveguide cavities: $L_{ris1}=L_{ris5}$=27.617; $L_{ris2}=L_{ris4}$=25.889; L_{ris3}= 25.881.

Note that in this case the first and last inverters are not replaced with the equivalent circuit in Fig. 7 (the reason will be clarified in Sec. V). The computed equivalent circuit is shown in Fig. 11 while the computed response is reported in Fig. 12 (solid lines).

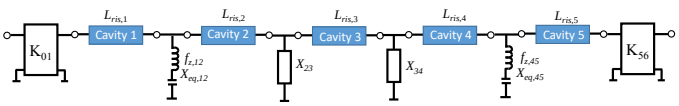

Fig. 11. Scheme of the filter equivalent circuit (second example).

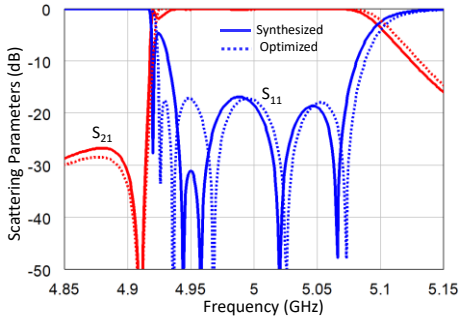

Fig. 12. Response of synthesized equivalent circuit (second example). Solid lines: synthesized circuit (Fig. 11). Dashed lines: response of the optimized circuit. Parameters of the optimized circuit: $L_{ris1}=L_{ris5}$=27.629; $L_{ris2}=L_{ris4}$=25.782; L_{ris3}= 25.820; $K_{01}=K_{56}$=0.379; $X_{23}=X_{34}$=0.0797.

We observe that the passband response obtained from the synthesized circuit (solid lines in Fig. 12) is in this case somewhat degraded with respect the ideal equiripple characteristic. This is mainly due to the normalized bandwidth (3.07%), noticeably larger than that in the first example, but

also other reasons contribute to the response degradation, such as the asymmetric assigned zeros, the small separation of TZs from the passband and the assigned position of the FVCs close to the external loads. In any case, the synthesized response is not too far from the desired one, which can be easily recovered by optimizing the parameters of the circuit in Fig. 11. To maintain unchanged the stopband response around the TZ frequency, we have not modified the parameters of the rejection resonators ($X_{eq,i,i+1}$ and $f_{z,i,i+1}$). The other parameters, obtained with a very fast circuit optimization, are reported in the caption of Fig. 12. The optimized response, also reported in Fig. 12 (dotted lines), is perfectly equiripple in the passband as required.

IV. DIMENSIONING OF THE FILTER

After the derivation of the equivalent circuit of the filter (Fig. 8), the next step, representing the filter dimensioning, consists in replacing the shunt-connected coupling reactances with suitable physical structures, implemented in rectangular waveguide.

Once these structures have been identified, we can dimension each of them separately, imposing the same S parameters of the synthesized blocks. To do this, we first represent the selected physical structures by means of the equivalent circuit shown in Fig. 13, composed by a shunt reactance between two sections of waveguide. Note that the equivalence holds true exactly for lossless structures.

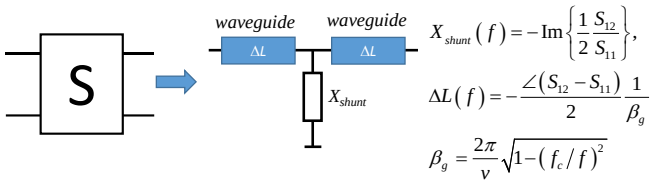

Fig. 13. Equivalent circuit of the coupling structures.

The parameters of the equivalent circuit are related to the S parameters of the 2-port coupling structure through the relationships shown in Fig. 13, consequently ΔL and X_{shunt} generally depend on the frequency. In case of approximately frequency independent couplings (e.g. the inductive irises) both X_{shunt} and ΔL are about constant in the filter passband and their value a f_0 can be used for representing the coupling. When instead FVCs are considered, the reactance X_{shunt} must behave like a series resonator, then exhibiting a strong dependence on the frequency. It can be observed that a weak dependence on f is instead presented by ΔL, for the structures implementing the FVCs here considered. From the physical point of view this means that these structures are about equivalent, at suitable reference sections, to a shunt-connected reactance. The length of the waveguide sections in Fig. 13 will be then assigned to $\Delta L(f_0)$ also for FVCs.

The dimensioning of each coupling structure is carried out by imposing that X_{shunt} extracted from the S parameters of the considered coupling structure, approximates at best, as the frequency varies, the corresponding reactance in the synthesized circuit (Fig. 8).

The parameter $\Delta L_{,i+1}$ of the dimensioned $(i,i+1)$ coupling structure adds up to the length of the adjacent cavities and represents the loading effect produced by the coupling. To compensate this effect, the cavities lengths $L_{ris,i}$ in the synthesized final circuit (Fig. 8) must by modified as follows:

$$L'_{ris,i} = L_{ris,i} - \left(\Delta L_{i-1,i} + \Delta L_{i,i+1}\right) \quad (10)$$

Note that this correction assumes $\Delta L_{,i+1}$ independent on the frequency. As this is true only in a first approximation, some adjustment of the lengths $L'_{i,i+1}$ may be necessary to get the expected passband response.

A. Coupling structures implementing the shunt reactances

The shunt reactances in Fig. 8 are either frequency-independent (no transmission zero introduced) or resonant (at the frequency of a transmission zero). In the former case, they can be implemented with classical inductive irises [20]. In the latter case, we need suitable discontinuities capable of producing a complete reflection at the frequency of the transmission zero and to present the required reactance value in the pass band. Such a behavior is exhibited by a partial-height post, which has been the first resonating coupling structure proposed in the literature for realizing waveguide filters with FVC [2], [4].

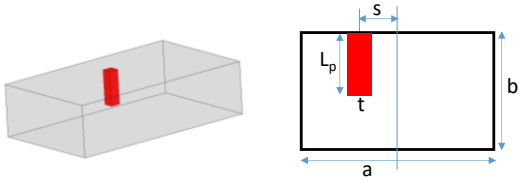

Fig. 14. Partial height post with square cross-section.

Fig. 14 shows the geometry of this discontinuity with the relevant geometric parameters.

The main advantage of the partial-height post is undoubtedly the compactness (it is all included inside the waveguide). On the other hand there is also a noticeable drawback, represented by the largest realizable value of the slope parameter ($X_{eq,i,i+1}$), which is relatively small. Consequently, the transmission zero cannot be placed too close to the passband. In fact, the closer the transmission zero to the passband, the larger the required slope parameter.

To overcome this limitation, the waveguide singlet can be used [21]-[26]. This structure is composed by an overmoded cavity, excited by the dominant mode of the input-output waveguides. This mode does not resonate in the cavity but can propagate from input to output, thus realizing a bypass coupling. A triplet configuration is then obtained, producing, in general, one transmission zero and one reflection zero. By a proper choice of the singlet dimensions, it has been demonstrated that the reflection zero can be pushed very distant from the transmission zero, realizing the so-called *stopband singlet* [25]. This type of singlet can be used as a resonating coupling in FVC waveguide filters. Fig. 15 shows two possible implementation of stopband singlets [25],[26].

The TE301 singlet adopts an overmoded cavity resonating on TE_{301} mode and it is a symmetric structure [25]. The second singlet in Fig. 10 [26] operates on TE_{201} mode and can be considered (in a first approximation) as a stub connected in parallel to the waveguide. The largest separation between reflection and transmission zeros is obtained with the TE301 singlet, which, however, is bigger than the TE201 singlet. Both structures allow large values for $X_{eq,i,i+1}$, so transmission zeros

placed very close to the filter passband. On the other hand, they are bulky and not suitable for small values of $X_{eq,i,i+1}$ (i.e. transmission zeros distant from the passband).

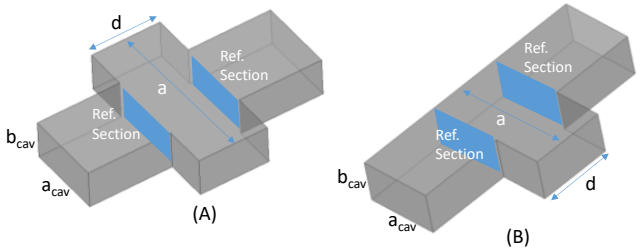

Fig. 15. (A) TE301 Singlet. (B) TE201 Singlet-stub

All the coupling structures above discussed can be represented by the equivalent circuit in Fig. 13 and, as said before, exhibit the parameter ΔL extracted from the equivalent circuit in Fig. 13 about constant in the filter passband.

In case of the inductive irises with assigned thickness, the evaluation of the aperture is performed by imposing the following condition at f_0:

$$X_{shunt}\left(f_0\right) = X_{i,i+1} \tag{11}$$

where $X_{i,i+1}$ are the frequency-independent reactances in the synthesized circuit (Fig. 8). The length $\Delta L_{i,i+1}$ is then evaluated from the equations in Fig, 13 for $f=f_0$.

In the case of FVC coupling structures (partial-height post or singlets), the shunt reactance X_{shunt} should approximate the lumped series resonator, resonating at the frequency $f_{z,i,i+1}$, with equivalent reactance $X_{eq,i,i+1}$. The dimensioning of the structure can then be achieved by imposing that the extracted reactance X_{shunt} satisfies the following conditions:

$$\begin{aligned} &X_{shunt}\left(f_{z,i,i+1}\right) = 0 \\ &X_{shunt}\left(f_0\right) = X_{eq,i,i+1}\left(\frac{f_0}{f_{z,i,i+1}} - \frac{f_{z,i,i+1}}{f_0}\right) \end{aligned} \tag{12}$$

The dimensioning accuracy can be evaluated by comparing $|S_{11}|$ and $|S_{12}|$ vs. frequency obtained from the dimensioned coupling structure with the same parameters computed from the synthesized lumped resonator.

Once each coupling structure has been dimensioned, the values of $\Delta L_{i,i+1}$ obtained from equations in Fig. 13 for $f=f_0$ allows correcting the loading effect introduced by the couplings structures on the adjacent cavities. However, the residual frequency dependence of $\Delta L_{i,i+1}$ in the filter passband may require an adjustment of the computed cavities lengths $L'_{i,i+1}$ obtained from (10).

B. *Example of filter dimensioning*

We show in the following how to realize the dimensioning of the filter introduced by first example in Section IIIC. We have to observe that this filter is part of a diplexer discussed in [28], where the design procedure for filters with FVCs here described was originally introduced. The work in [28] is however focused on the diplexer design and few details are given about the design of the filters composing the diplexer.

The rectangular waveguide used for both the cavities and the input/output lines has the following dimensions of the cross section: a_{cav}=12.95mm, b_{cav}=8.5mm. The cavities resonate on TE_{102} mode (n=2).

The constant reactances X_{01}, X_{12}, X_{34}, X_{56}, X_{67} in the final equivalent circuit of the filter (Fig. 9) have been implemented by inductive irises with thickness t=1mm. The result of the dimensioning, carried out as previously described, has produced the following values for the irises apertures (in mm): W_{01}=5.461, W_{12}=3.58, W_{34}=3.456 W_{56}=3.572, W_{67}=5.461. The corresponding value of $\Delta L_{i,i+1}$ evaluated at f_0 result (in mm): ΔL_{01}=0.302, ΔL_{12}=0.183, ΔL_{34}=0.174, ΔL_{56}=0.182, ΔL_{67}=0.302. The singlet operating on TE_{301} mode (Fig. 15A) has been chosen as resonating coupling structures since they allow to realize the relatively large slope parameter required by the equivalent resonators ($X_{eq,i,i+1}$). The dimensioning of the singlets has been carried out by imposing the conditions (12). With reference to Fig. 15A, the dimensioned singlets have the following dimensions (mm): a_{23}=32.333, d_{23}=9.723, a_{45}=32.059, d_{45}=9.534. To give an idea of the dimensioning accuracy, Fig. 16 shows $|S_{11}|$ and $|S_{12}|$ of the dimensioned singlets (using a mode matching based full wave simulator), compared with the same parameters obtained from the synthesized lumped resonators.

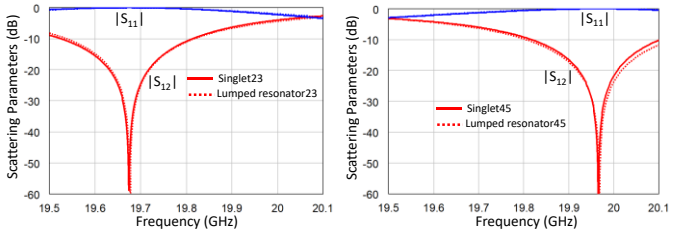

Fig. 16. Evaluated S parameters of dimensioned TE301 singlets (solid lines). Dotted lines refer to $|S_{11}|$ and $|S_{12}|$ of the syntesized lumped resonators.

The values of the lengths $\Delta L_{i,i+1}$ extracted from the singlets model are: ΔL_{23}=5.225mm, ΔL_{45}=5.105mm. To confirm the relatively small dependence of these lengths on the frequency we report in Fig. 17 the quantity $(\Delta L_{i,i+1}(f)-\Delta L_{i,i+1}(f_0))$.

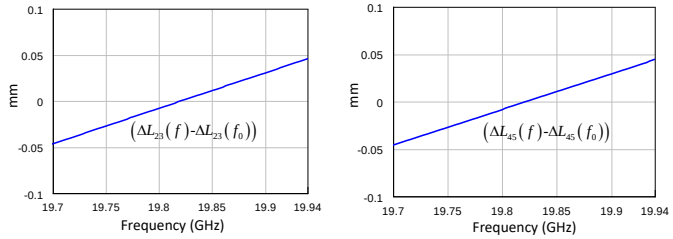

Fig. 17 Variation of the lenghts $\Delta L_{i,i+1}$ with respect the value at f_0 for the dimensioned singlets

As you can see, the variation of $\Delta L_{i,i+1}$ in the passband for both the singlets is less than ±0.05mm. This confirms the assumption on the frequency independence of the waveguide sections lengths in the equivalent circuit of the singlets (Fig. 13).

The final step of dimensioning consists in the evaluation of the corrected cavities length by means of (10). The following values (in mm) are obtained: L'_{ris} = [17.222, 13.016, 13.011, 13.233, 13.174, 17.225].

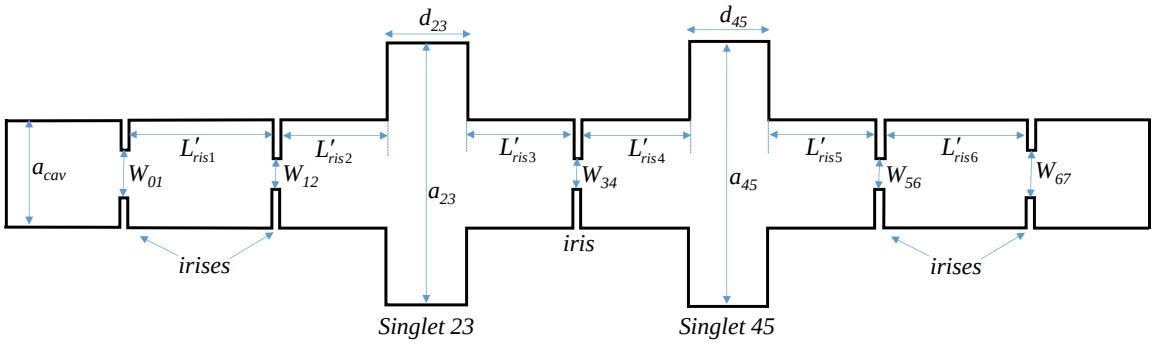

Fig. 18. Top view drawing of the dimensioned filter. The irises thickness is 1 mm. The height of the structure is b_{cav}=8.5 mm

Fig. 18 shows the top view drawing of the filter with all relevant dimensions.

The filter response computed through full-wave simulation (mode matching) is shown in Fig. 19 (solid lines). For reference, the ideal Chebycheff characteristic of the synthesized filter is also reported on the graph (dashed lines). Although some discrepancies can be observed, it must be remarked that no optimization has been employed after the initial dimensioning. In any case, the dimensioning can be further improved with numerical optimization (that is very fast in this case because the starting point is close to the desired goal). An optimization has been carried using the same full-wave modelling used for the analysis of the filter. Few iterations have been required to obtain the response shown in Fig. 19 (dotted lines), which is practically indistinguishable from the ideal response in the passband.

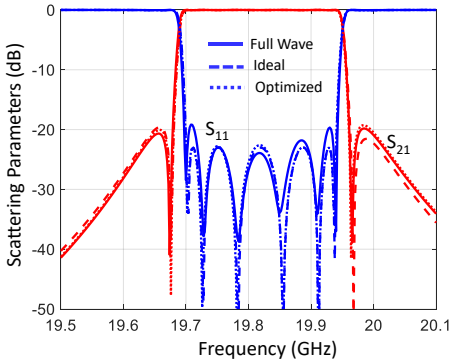

Fig. 19. Simulations of the waveguide filter (S_{11} & S_{22}). Solid lines: Dimensioned filter response. Dashed lines: Ideal Chebycheff characteristic. Dotted lines: Optimized filter response.

V. EXPERIMENTAL VALIDATION

To validate the novel design approach, a filter in SIW technology [29]-[31], designed with the procedure described in this work, has been manufactured. The filter requirements, together with the characteristics of the selected substrate are reported in Table I. Note that two coincident transmission zero are imposed at the specified frequency.

For the synthesis of the low-pass prototype, the passband limits have been slightly increased (4.9245-5.078 GHz) to introduce a safety margin. The synthesis of the filter equivalent circuit has been described in Section IIIC (second example), resulting in the scheme in Fig. 11. We recall that standard rectangular waveguide cavities filled with a lossless dielectric material (ε_r=2.2) have been assumed in the synthesis. The cross-section dimensions are a_{cav}=30mm, b_{cav}=1.524mm.

TABLE I
TEST FILTER SPECIFICATIONS

Passband	4.925-5.075 GHz
Return Loss	17 dB
Filter order	5
Transmission zeros	4.91 GHz (2)
Substrate Thickness	1.524 mm
Substrate ε_r	2.2 (nominal)
Substrate Manufacturer	Taconic (TLY-5)
Input-output port	Coaxial

It can be observed that the synthesized circuit is symmetric. The first and last couplings are modeled as ideal inverters because they will be implemented by a waveguide-to-coaxial transition suitably dimensioned.

The dimensioning of the filter consists in the replacement of the elements in the equivalent circuit (Fig. 11) with corresponding SIW structures. The side walls of classical waveguide components are implemented in SIW technology by means of via holes with diameter d_{via}=1 mm and separation $s_{via} \approx 2$ mm.

The rectangular waveguide connecting the elements in Fig. 11 is accurately represented by an equivalent SIW structure [29] with a_{SIW}=30.6 mm (distance between the vias center).

The shunt-connected series resonators in Fig. 11 (identical) have been implemented by H-plane stubs, modelled as a stopband singlet operating on the TE_{201} mode (Fig. 15B). The dimensioning of the singlet was realized by imposing the resonance frequency and the equivalent reactance extracted from X_{shunt} (equivalent circuit in Fig. 13) equal to those of the series resonators in the final equivalent circuit of the filter (Fig. 11). The S parameters of the SIW singlet have been computed by means of full wave simulation (to this aim, the commercial software HFSS was used). The singlet dimensions obtained are a=59.38 mm and d=25.05 mm. Fig. 20 shows the comparison between the scattering parameters from the ideal resonator and the physical SIW structure (the SIW geometry is also reported). The extracted equivalent circuit of the dimensioned singlet allows the evaluation of the waveguide lengths ΔL of the equivalent circuit (Fig. 13). The correction to be applied to the

cavities length results Δ_{ST}=12.93 mm. Note that in this case the frequency dispersion of Δ_{ST} around f_0 is about ±0.45mm then some adjustment of the initially dimensioned filter will be necessary.

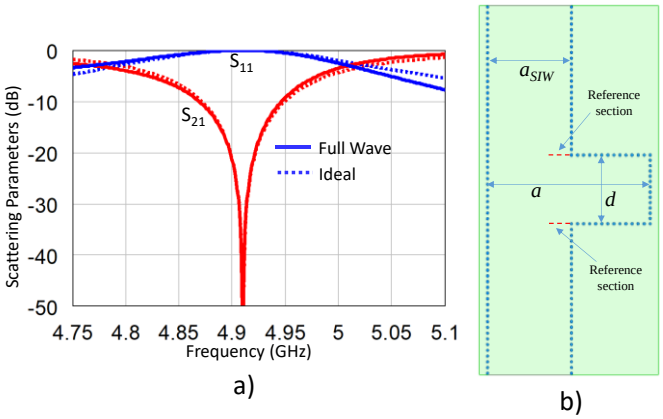

Fig. 20. a) S parameters of the Stopband Singlet. Solid lines: HFSS Simulation of the SIW structure. Dotted lines: ideal response (lumped series resonator with X_{eq}=10.437, f_z=4.91 GHz). b) Geometry of the singlet in SIW.

The following elements to be physically implemented are the ideal inverters at filter input and output. These are realized by the SIW-to-coaxial transition shown in Fig. 21. The dimensioning of the transition has been carried out by requiring S_{22} (SIW port) equal to $S_{22}=\left(K_{01}^2-1\right)/\left(K_{01}^2+1\right)=-0.7488$, with K_{01}=0.379 value of the inverter parameter in the designed filter (circuit in Fig. 11). Imposing this result at the passband center frequency the geometric parameters in Fig. 21 have been determined: P_X=14.961 mm, P_Y=5.446 mm and Δ_{SC}=-3.714 mm. The last parameter (Δ_{SC}) represents the displacement of the SIW reference section with respect to the coaxial axis, required to fit the phase of S_{22} (180°)

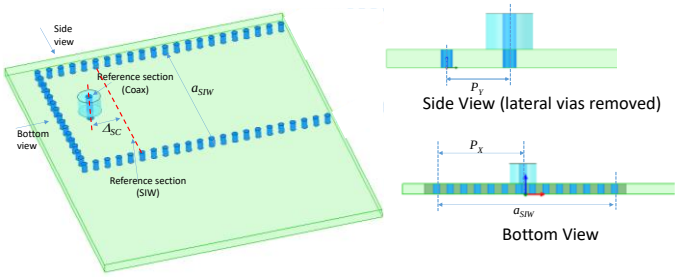

Fig. 21. SIW-to-coax transition. The inner and outer radius of the coaxial termination are r_{in}=0.6 mm, r_{out}=2 mm (Z_c=50 Ω). The coaxial termination is filled with the teflon (ε_r=2.1). Simulations was carried out by HFSS.

The last components to be realized are the two frequency-independent reactances X_{23}=X_{34}=0.0797, which have been implemented with inductive irises (Fig. 22). Imposing the same magnitude of S_{11} of the ideal reactance and the physical structure, the aperture size W_{23}=9.14 mm has been found. The corresponding value of the parameter ΔL of the equivalent circuit results: Δ_I =-0.374 mm (note that here the reference sections are represented by the iris axis).

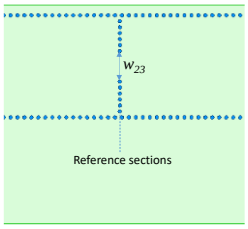

Fig. 22. SIW Iris (dimensions not in scale)

The SIW filter is obtained by connecting the dimensioned elements through waveguide sections. The geometry obtained is shown in Fig. 23, where all the relevant dimensions are reported.

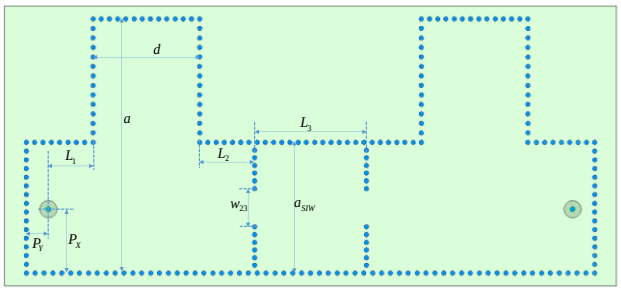

Fig. 23. Geometry of the designed SIW filter. All dimensions are assumed with respect to the axis of the vias. The vias diameter is 1mm and the pass is (about) 2 mm. As the structure is symmetrical, dimensions are specified for only one half.

Taking into account the loading produced by the coupling structures on the cavities, the lengths of the connecting waveguides (L_1, L_2, L_3 in Fig. 23) are obtained as follows:

$$L_1=L_5=L_{ris,1}+\Delta_{SC}-\Delta_{ST},\quad L_2=L_4=L_{ris,2}-\Delta_I-\Delta_{ST},\quad L_3=L_{ris,3}-2\Delta_I \tag{13}$$

The waveguides lengths ($L_{ris,1}$, $L_{ris,2}$, $L_{ris,3}$) are those in the final equivalent circuit of the filter and are reported in the caption of Fig. 12. All the dimensions of the initially designed SIW filter are reported in the first column (*Initial*) of Table II.

TABLE II
COMPUTED PARAMETERS OF THE SIW FILTER (MM)

	Initial	*Tuned*	*HFSS*
L_1	10.985	11.026	10.49
L_2	13.226	13.226	12.91
L_3	26.568	26.522	26.26
P_X	14.961	14.961	14.961
P_Y	5.446	5.446	5.2
a	59.38	59.38	59.5
d	25.05	25.05	25.05
w_{23}	9.14	9.14	8.99

The dimensioned filter can be verified in a circuit simulator by representing the blocks dimensioned separately (coax-SIW transition, singlet and iris) with their scattering parameters (referred to the dominant mode only). The SIW lines are represented with the equivalent rectangular waveguide (same height b and equivalent width a_{eq}=30 mm), operating on TE_{10} mode. Fig. 24 shows the computed response (solid lines).

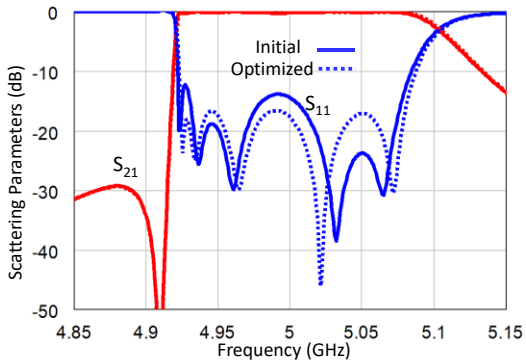

Fig. 24. Computed circuit response (S_{11} and S_{21}) of the SIW filter based on the computed S parameters of the composing blocks. Solid lines: initial cavities length from (13). Dotted lines: tuned lengths.

As can be observed, the passband response is somewhat distorted due to the frequency dispersion of the correcting factors $\Delta L_{i,i+1}$. The distortion can be however easily reduced by tuning the lengths of the connecting waveguides (L_1, L_2, L_3) in a circuit simulator. Table II reports in the second column *(Tuned)* the lengths values after the fine tuning (the other parameters are unchanged). The response of the tuned filter (Fig. 24, dotted lines) is now equiripple in the passband.

The whole SIW structure has been also analyzed with a full wave simulator (HFSS) and the geometrical parameters have been further tuned to get the computed response as close as possible to the one in Fig. 24. The applied corrections are however relatively small, as confirmed by the values reported in Table II (column *HFSS*). Fig. 25 shows the comparison between the full wave simulation of the SIW filter with the adjusted dimensions and the optimized response based on the cascaded-block model of the filter (Fig. 24).

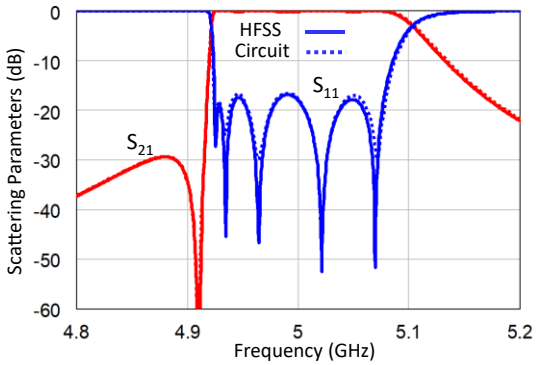

Fig. 25. Full-wave response (S_{11} and S_{21}) of the dimensioned SIW filter (solid lines). For comparison, also the circuit response from Fig. 24 is reported.

It is worth remarking that the new design procedure implements the dimensioning of the filter element by element, with each element (physical coupling structure) described by the S parameters referring only to the dominant mode. When the interactions among the blocks due to the higher order modes are not negligible (as happens in the case of the SIW filter), a final adjustment of the design based on full wave analysis is necessary.

To experimentally validate the proposed design approach, the SIW filter has been finally fabricated. The ports of the filter were implemented by two SMA coaxial probes, directly inserted in the SIW guide section. The TLY-5 laminated substrate was adopted (ε_r=2.20, tanδ=0.0009, thickness=1.524 mm). The metal vias were drilled using a CNC milling machine, and then metallized by using a silver-based conductive paste (LPKF ProConduct®).

The measured response of the fabricated prototype is shown in Fig. 26, compared with the simulated response from HFSS. Note that dissipation losses are included in HFSS simulation by assigning the copper conductivity to all conductors and taking into account the nominal tanδ of the dielectric. A photo of the fabricated filter is reported in the inset of the Fig. 26.

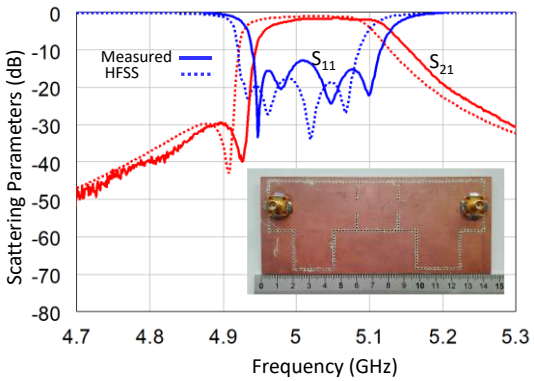

Fig. 26. Measured response (S_{11} and S_{21}) of the fabricated SIW prototype (solid lines). The full-wave response computed with HFSS (including losses) is reported for comparison. A photo of the fabricated filter is shown in the inset of the figure.

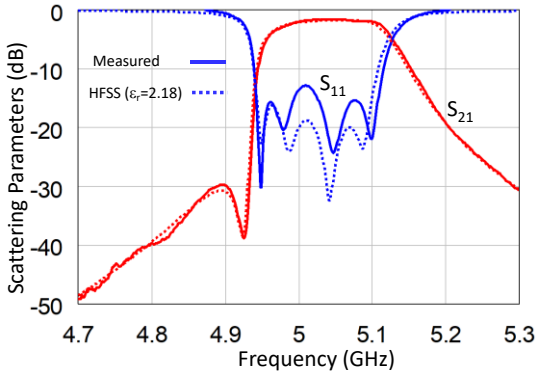

Fig. 27. Measured response (S_{11} and S_{21}) of the fabricated SIW prototype (solid lines) compared to HFSS simulation with ε_r=2.18 and lossy vias (conductivity $\sigma=3.5\cdot10^5$ S/m).

By observing Fig. 26, it is evident a displacement of the measured response by 20 MHz upward with respect to the simulated curves. We have attributed this frequency shift to the actual value of the relative dielectric permittivity of the substrate used in the manufactured prototype (the value declared by the manufacturer is in fact ε_r=2.2±0.02). To verify this hypothesis, the filter has been simulated again by assigning ε_r=2.18 to the permittivity of the substrate. Moreover, the conductivity of the vias was set to $\sigma=3.5\cdot10^5$ S/m, to account for the additional losses produced by the actual material used in the vias fabrication. Fig. 27 shows the result of the HFSS

simulation compared again with the measurements. In this case, no frequency shift can be observed between measured and simulated response.

With the corrected value of permittivity, it can be noted that the expected frequency of the transmission zero is perfectly confirmed by the measurements. Regarding the passband return loss, a certain degradation of the measurements with respect to the expected target can be observed. The most likely reason is the not perfect realization of the coax-to-waveguide transition.

Finally, the measured insertion loss is about 1.64 dB at the passband center frequency (5.02 GHz), practically coincident with the value obtained from the simulation. Note that, assuming the measured loss all due to the unload quality factor Q_0 of the SIW cavities, it results the value Q_0=420.

VI. CONCLUSIONS

In this work, a new procedure for the design of inline waveguide filters with up to *N*-1 transmission zeros (*N* number of resonators) has been presented. The zeros are introduced by means of resonant couplings that can be realized with various coupling structures (partial height posts, resonant irises, singlets). The proposed design procedure starts with the synthesis of a low pass prototype including frequency-dependent inverters. The prototype is then de-normalized by exploiting the coupling coefficient concept; using a sequence of circuit transformations, an equivalent circuit is finally derived, constituted by waveguide sections separated by shunt connected reactances, either frequency-independent or resonating (the latter introduce the transmission zeros). It is also described how to implement the shunt-connected resonating reactances by real structures, taking into account the loading effects they produce on the adjacent resonators.

Incidentally, it could be observed that the filters obtained with the novel procedure are structurally similar to extracted-pole filters [32]. There is, however, a fundamental difference: in extracted-pole filters TZs are introduced by the main cavities together with the poles. This makes their practical design and realization more difficult and critical. Moreover, the resulting structure is, in general, of larger size with respect to the same filter realized with FVCs.

The application of the proposed design procedure (particularly effective when the transmission zeros are close to the passband) has been illustrated in detail through the design of a waveguide filter in *Ka* band with two transmission zeros realized by stopband singlets. The experimental validation of the procedure has been finally carried out with the design and fabrication of an SIW filter operating at 5 GHz, with two coincident transmission zeros very close to the passband.

REFERENCES

[1] W. Meng, H. Lee, K. A. Zaki and A. E. Atia, "Synthesis of multi-coupled resonator filters with frequency-dependent couplings" in *IEEE MTT-S Int. Dig.*, Anaheim, CA, 2010, pp. 1716-1719.

[2] S. Amari and J. Bornemann, ``Using frequency-dependent coupling to generate finite attenuation poles in direct-coupled resonator bandpass filters," *IEEE Microw. Guided Wave Lett.*, vol. 9, no. 10, pp. 404-406, Oct. 1999.

[3] S. Amari, J. Bornemann, W. Menzel and F. Alessandri, "Diplexer design using pre-synthesized waveguide filters with strongly dispersive inverters," in *IEEE MTT-S Int. Dig.*, Phoenix, AZ, May 2001, pp. 1627-1630.

[4] M. Politi and A. Fossati, "Direct coupled waveguide filters with generalized Chebyshev response by resonating coupling structures," *Proc. 40th Eur. Microw. Conf. (EuMC)*, pp. 966–969, Paris, Sep. 2010.

[5] U. Rosenberg, S. Amari and F. Seyfert, "Pseudo-elliptic direct-coupled resonator filters based on transmission-zero-generating irises", in *Proc. Eur. Microw. Conf. (EuMC)*, pp. 962-965, 2010-Sep.

[6] A. Jedrzejewski, N. Leszczynska, L. Szydlowski and M. Mrozowski, "Zero-Pole Approach To Computer Aided Design of In-Line SIW Filters with Transmission Zeros," *Prog. Electromag. Resear.*, vol. 131, pp. 517–533, 2012.

[7] L. Szydlowski, A. Lamecki, and M. Mrozowski, "Coupled-resonator filters with frequency-dependent couplings: Coupling matrix synthesis," *IEEE Microw. Wireless Compon. Lett.*, vol. 22, no. 6, pp. 312–314, Jun. 2012.

[8] L. Szydlowski, A. Lamecki, and M. Mrozowski, "Coupled-resonator waveguide filter in quadruplet topologywith frequency-dependent coupling—A design based on coupling matrix," *IEEE Microw. Wireless Compon. Lett.*, vol. 22, no. 11, pp. 553–555, Nov. 2012.

[9] L. Szydlowski, N. Leszczynska and M. Mrozowski, "Generalized Chebyshev Bandpass Filters With Frequency-Dependent Couplings Based on Stubs," *IEEE Trans. Microw. Theory Techn.*, vol. 61, no. 10, pp. 3601-3612, Oct. 2013.

[10] L. Szydlowski, A. Jedrzejewski, andM.Mrozowski, "A trisection filter design with negative slope of frequency-dependent cross coupling implemented in substrate integrated waveguide (SIW)," *IEEE Microw. Wireless Compon. Lett.*, vol. 23, no. 9, pp. 456–4581, Sep. 2013.

[11] L. Szydlowski and M. Mrozowski, "A self-equalized waveguide filter with frequency-dependent (resonant) couplings", *IEEE Microw. Wireless Compon. Lett.*, vol. 24, no. 11, pp. 769–771, Nov. 2014

[12] L. Szydlowski, N. Leszczynska, A. Lamecki, and M. Mrozowski "Dimensional Synthesis of Coupled-Resonator Pseudoelliptic Microwave Bandpass Filters With Constant and Dispersive Couplings" *IEEE Trans. Microw. Theory Techn.*, Vol. 62, n.8, pp. 1634-1646, August 2014

[13] J. Kuo,Y. Wang, J. Kuo, "Diplexer with trisections synthesized by frequency-dependent coupling", in *Proc. Asia-Pacific Microwave Conf. (APMC)*, Vol. 3, pp. 1-3, Dec. 2015

[14] Q. Liu, D. Zhou, D. Zhang and Dalong Lv, "A Novel Frequency-Dependent Coupling With Flexibly Controllable Slope and Its Applications on Substrate-Integrated Waveguide Filters," *IEEE Microw. Wireless Compon. Lett.*, vol. 28, no. 11, pp. 993-995, Nov. 2018

[15] S. Tamiazzo and G. Macchiarella, "Synthesis of cross-coupled filters with frequency-dependent couplings," *IEEE Trans. Microw. Theory Techn.*, vol. 65, no. 3, pp. 775–782, Mar. 2017.

[16] Y. He, G. Macchiarella, G. Wang, L. Sun, L. Wang and R. Zhang, "A Direct Matrix Synthesis for In-Line Filters With Transmission Zeros Generated by Frequency-Variant Couplings" *IEEE Trans. Microw. Theory Techn.*, vol. 66, N. 4, pp. 1780-1789, April 2018

[17] Y. He, G. Macchiarella, Z. Ma, L. Sun and N. Yoshikawa, "Advanced direct synthesis approach for high selectivity in-line topology filters comprising N-1 adjacent frequency-variant couplings" *IEEE Access*, vol. 7, pp. 41659-41668, Mar. 2019

[18] P. Zhao and K. Wu, "Cascading fundamental building blocks with frequency-dependent couplings in microwave filters," *IEEE Trans. Microw. Theory Techn.*, vol. 67, no. 4, pp. 1432–1440, Apr. 2019.

[19] Y. Zhang, H. Meng and K. Wu, "Direct Synthesis and Design of Dispersive Waveguide Bandpass Filters," *IEEE Trans. Microw. Theory Techn.*, vol. 68, no. 5, pp. 1678-1687, May 2020.

[20] G. L. Matthaei, L. Young, and E. M. T. Jones, *Microwave FilterImpedance Matching Networks and Coupling Structures*. New York: McGraw-Hill, 1964.

[21] M. Guglielmi, P. Jarry, E. Kerherve, O. Roquebrun and D. Schmitt, "A new family of all-inductive dual-mode filters," *IEEE Trans. Microw. Theory Techn.*, vol. 49, no. 10, pp. 1764-1769, Oct. 2001.

[22] S. Amari and U. Rosenberg, "Characteristics of cross (bypass) coupling through higher/lower order modes and their applications in elliptic filter design" *IEEE Trans. Microw. Theory Techn.*, vol. 53, no. 10, pp. 3135–3141, Oct. 2005.

[23] S. Bastioli, "Nonresonating Mode Waveguide Filters", *IEEE Microwave Mag.*, vol. 12, no. 6, pp. 77–86, Oct. 2011.

[24] M.M. Mendoza, D. M. Martinez, D. C. Rebenaque and A. Alvarez-Melcon, "Enhanced topologies for the design of dual-mode filters using inductive waveguide structures", *Radio Sci., 50*, 66–77, 2012

[25] G. Macchiarella, G. Gentili, and L. Accatino, “Stopband Singlet: A Novel Structure Implementing Resonating Couplings,” *IEEE Microw. Wireless Compon. Lett.*, vol. 30, no. 5, pp. 473-476, May 2020.

[26] G. Macchiarella et al., "Accurate Modeling of Stubs Used as Resonant Coupling Elements in SIW Filters", *IEEE Microw. Wireless Compon. Lett.*, vol. 30, no. 12, pp. 1125-1128, Dec. 2020

[27] S. Bastioli and R. V. Snyder, "Non-resonating Modes Do It Better!: Exploiting Additional Modes in Conjunction With Operating Modes to Design Better Quality Filters," *IEEE Microw. Mag.*, vol. 22, no. 1, pp. 20-45, Jan. 2021.

[28] G. Macchiarella, G.G. Gentili, L. Accatino, and V. Tornielli di Crestvolant, “A Synthesis-based Design Procedure for Waveguide Duplexers Using a Stepped E-plane Bifurcated Junction” *IEEE MTT-S International Microwave Symposium*, Los Angeles, CA, USA, Jun 21–26, 2020.

[29] M. Bozzi, A. Georgiadis, and K. Wu, “Review of Substrate Integrated Waveguide (SIW) Circuits and Antennas,” *IET Microwaves, Antennas and Propagation*, Vol. 5, No. 8, pp. 909-920, June 2011.

[30] X. Chen and K. Wu, “Substrate Integrated Waveguide Filter: Basic Design Rules and Fundamental Structure Features,” *IEEE Microwave Magazine*, vol. 15, no. 5, pp. 108-116, July-Aug. 2014.

[31] K. Wu, M. Bozzi, and N. J. G. Fonseca, “Substrate Integrated Transmission Lines: Review and Applications,” *IEEE Journal of Microwaves*, Vol. 1, No. 1, Jan. 2021.

[32] G. Macchiarella, G.G. Gentili, C. Tomassoni, S. Bastioli, R.V. Snyder, “Design of Waveguide Filters With Cascaded Singlets Through a Synthesis-Based Approach” *IEEE Trans. Microw. Theory Techn.*, vol. 68, no. 6, pp. 2308-2319, June 2020